Journal of Ceramic Processing Research. Vol. 21, No. 3, pp. 351~357 (2020)
(Received 5 December 2019, Received in revised form 6 March 2020, Accepted 9 March 2020)
https://doi.org/10.36410/jcpr.2020.21.3.351

J O U R N A L O F
Ceramic Processing Research

Fabrication of ZrB_2/SiC/WC composites via spark plasma sintering and enhancement of oxidation resistance

Jae-Seok Choi[a,], Jung-Hun Kim[b,**], Jae Uk Hur[a], Sung-Churl Choi[a] and Gye-Seok An[a,*]**
[a]*Division of Materials Science and Engineering, Hanyang University, 222 Wangsimni-ro, Seongdong-gu, Seoul 04763, Korea*
[b]*Ceramicware Technology Center, Korea Institute of Ceramic Engineering & Technology, 3321 Gyeongchung-daero, Sindun-myeon, Icheon 17303, Korea*

To prevent the oxidation of ultra-high-temperature ceramic zirconium diboride (ZrB_2) at high temperatures, this study fabricated sintered composites containing silicon carbide and tungsten carbide, and examined the properties related to high-temperature oxidation. Spark plasma sintering was employed for rapid sintering, and a high-temperature torch test was conducted on samples to determine their surface oxidation behaviour. The composites oxidised at high temperature showed different surface oxidation behaviour according to the type of carbide-based additive. Composites containing both carbides, which have different oxidation mechanisms, exhibited better resistance to oxidation than those containing a single carbide.

Keywords: ZrB_2, SiC, WC, Spark plasma sintering, Oxidation resistance.

Introduction

In general, ceramic materials tend to melt or decompose at temperatures higher than 3,000 °C. However, ultra-high-temperature ceramics (UHTCs) are known for their melting points above 3,000 °C, high chemical stability, and excellent resistance to oxidation. UHTCs are group IV, V, and VI transition metals such as boride, carbide, nitride, including TaB_2, HfC, and BN [1, 2]. The term UHTC was proposed in 2004 during a joint workshop between the National Science Foundation of the United States and the Air Force Office of Science Research. UHTCs have been extensively studied as materials for extreme environments such as space shuttles, transonic airliners, and rocket propulsion systems [3].

Zirconium diboride (ZrB_2), a covalent material with hexagonal crystal structure, is a representative UHTC along with TiB_2 and HfB_2. ZrB_2 has a melting point higher than 3,200 °C, Young's modulus of 490 GPa, and hardness of at least 20 GPa. It also offers excellent thermal and electrical conductivity. Among UHTCs, ZrB_2 has relatively low density and excellent strength at high temperatures, making it an ideal material for aerospace and next-generation energy devices [4, 5]. Despite these advantages, the material has limited applications in extreme environments owing to its poor durability against surface oxidation at high temperatures. When oxidised in air, oxide is produced in two phases on the surface of ZrB_2, the states of which change with temperature. First, a B_2O_3 layer has been observed on the surface at temperatures below 1,000 °C, with a porous ZrO_2 layer beneath it; the pores are filled with B_2O_3. When the temperature increases further, the B_2O_3 glass layer is liquefied and vaporises at approximately 1,300 °C, and the space that was occupied B_2O_3 becomes a path for oxygen from the atmosphere to enter, which accelerates the oxidation of ZrB_2 [6-9]. The chemical equations describing this oxidation process are as follows.

$$2ZrB_2 + 5O_2 \rightarrow 2ZrO_2 + 2B_2O_3$$

$$B_2O_3(l) \rightarrow B_2O_3(g)$$

To prevent the above oxidation reactions, researchers are studying oxidation-resistant ZrB_2 composites, especially ZrB_2-SiC and ZrB_2-WC. In the ZrB_2-SiC composite, B_2O_3 binds with SiO_2 to form a borosilicate layer which, in contrast to pure ZrB_2, prevents B_2O_3 from becoming porous owing to volatilisation. However, B_2O_3 shifts to the surface when volatilised, and pulls SiO_2 existing in liquid phase to the surface layer. The surface becomes rich with SiO_2, and a layered structure rich in ZrO_2 develops within the composite, leading to separation of the borosilicate surface layer [10-17].

In the case of the ZrB_2-WC composite, WC is oxidised into WO_3, and the particles experience volumetric expansion during this process. The compressive stress acting between the particles blocks the path of oxygen, thus interfering with the oxidation of the composite [18-22]. The purpose of this study is to enhance oxidation resistance by combining the two abovementioned

*Corresponding author:
Tel : +82-2220-0505
Fax: +82-2290-6767
E-mail: faustmaro@hanyang.ac.kr
**These arthurs were contributed equally to this work.

advantages, i.e., blocking the path of liquid-phase SiO_2 due to volumetric expansion of WO_3 oxidised from WC, and preventing oxygen infiltration by the glass layer formed on the surface during the oxidation of SiC composites. This study sintered ZrB_2-SiC-WC and compared its oxidation resistance to those of pure ZrB_2, ZrB_2-SiC, and ZrB_2-WC.

Experiment

The materials used in the experiment were commercial powder ZrB_2 (99.5%, 1-2 μm, APS powder, Alfa Aesar), SiC (99.8%, 1 μm, S.A. 11.5 m^2/g beta-phase, Alfa Aesar), and WC (99%, 2 μm, Sigma-Aldrich). Composites with four different compositions were prepared using ZrB_2 as a base. The composites are referred to as Z, ZS, ZW, and ZSW according to their compositions. The four batches are presented in Table 1. Powder samples from each batch were placed in a Nalgene bottle with methanol and subjected to ball milling for 24 h using WC media. The mixed powders were collected via rotary expansion and dried for 24 h in a vacuum dryer, followed by sieving using a 100-mesh sieve. The powders were then subjected to spark plasma sintering. The furnace had a vacuum atmosphere (under 2×10^{-2} mmHg), and the sintering temperature was raised at a rate of 100 °C/min. Sintering was performed for 15 min at 1,800 °C and 30 MPa for Z and ZS, and for 15 min at 1,900 °C and 60 MPa for ZW and ZSW. The sintering conditions for each composition are listed in Table 2. During sintering, carbon paper was used to prevent reactions with the mould and punch, and to facilitate separation. The sample surfaces were polished with sandpaper to remove any traces of carbon paper after sintering. The sintered pellets were disc-type with a diameter of 10 mm and thickness of 2 mm. The density of each pellet was measured by Archimedes' principle, and the relative density was obtained by calculating the theoretical density based on the rule of mixtures. Torch oxidation was performed to determine differences in oxidation among pellets. The gases used in the experiment were propane gas and oxygen gas. The gas flow rate was adjusted to maintain the flame temperature, which was measured with a pyrometer, at 1,600 °C. The pellets were placed on a refractory material to withstand flames at high temperature, and a pellet-shaped holder was made to prevent the pellets from moving about due to the strong flames. The experimental setup for torch oxidation and a photograph of the actual experiment are presented in Fig. 1. Thermal gravimetric analysis (TGA; TA Instruments SDT Q600, USA) was conducted to determine the changes in sample mass during oxidation at high temperatures under atmospheric pressure. To analyse the phase of each pellet, X-ray diffraction (XRD, Rigaku, Tokyo, Japan, using CuKa radiation) was used to scan the samples at 2° per minute in the range of 2Θ = 20-80°. The oxidation of composites was examined by applying field-emission scanning electron microscopy (FE-SEM; JEOL JSM-6700, Japan) and energy-dispersive spectroscopy (EDS; BRUKER AXS) to the cross-sections.

Table 1. Compositions of samples Z, ZS, ZW, and ZSW.

Samples	Composition (mol%)		
	ZrB_2	SiC	WC
Z	100		
ZS	73	27	
ZW	94		6
ZSW	73	21	6

Table 2. Spark plasma sintering conditions of samples.

Samples	Sintering condition			
	Temperature (°C)	Pressure (MPa)	Time (min)	Relative density (%)
Z	1800	30	15	97.9
ZS	1800	30	15	97.8
ZW	1900	60	15	98.2
ZSW	1900	60	15	98.6

Results

In Fig. 2, the photographs on the left and right were taken before and after the torch oxidation experiment, respectively. The surfaces of the sintered samples were polished. As such, the surfaces before the torch oxidation experiment had a metallic shine. Fig. 2(a) shows the sample with sintering of only ZrB_2. The sample on the right has a largely oxidised surface with ash-grey colour after the torch oxidation experiment. Separation was observed on the surface layer. Because of oxidation, only porous ZrO_2 remained on the surface layer; the layer separation can be traced to the decrease in strength. Fig. 2(b) shows the ZrB_2-SiC composite. The photograph, taken after the torch oxidation experiment, shows that the sample has lost its metallic shine but appears to have a shiny coating. SiC undergoes oxidation to form SiO_2, while ZrB_2 forms B_2O_3, thus resulting in borosilicate. Fig. 2(c) shows the ZrB_2-WC composite; the sample after the torch oxidation experiment has a surface similar to that of Sample Z; however, the surface layer separation observed for Sample Z did not occur. WC produces WO_3 when oxidised, and WO_3 is believed to have filled the space between the porous ZrO_2 layers in Sample Z. Fig. 2(d) shows the ZrB_2-SiC-WC composite, which is similar to Sample ZS in terms of surface and other properties.

Fig. 3 shows XRD patterns of Z, ZS, ZW, and ZSW composites before and after the torch oxidation experiment. In the XRD patterns in Fig. 3(a), ZrB_2, SiC, and WB peaks are marked with circles, triangles, and squares, respectively. In all four XRD patterns, the phases of ZrB_2 can be determined. The composites

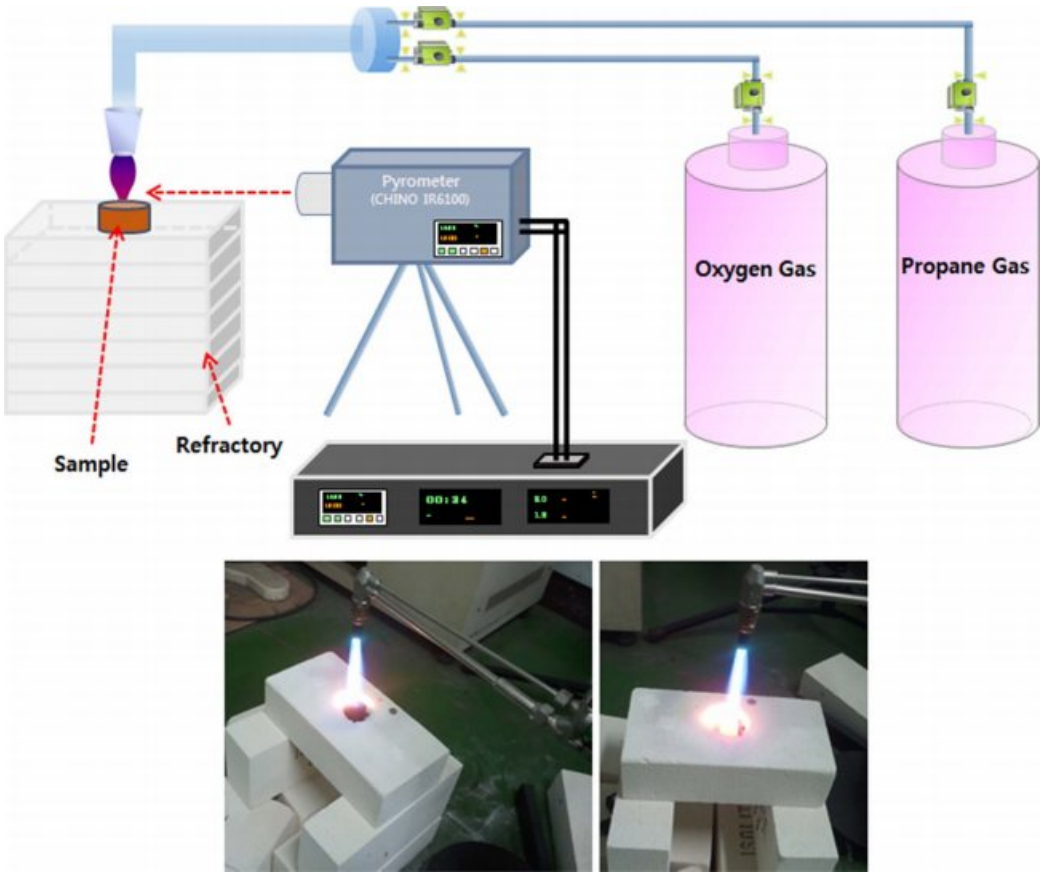

Fig. 1. Experimental setup for torch oxidation and photographs.

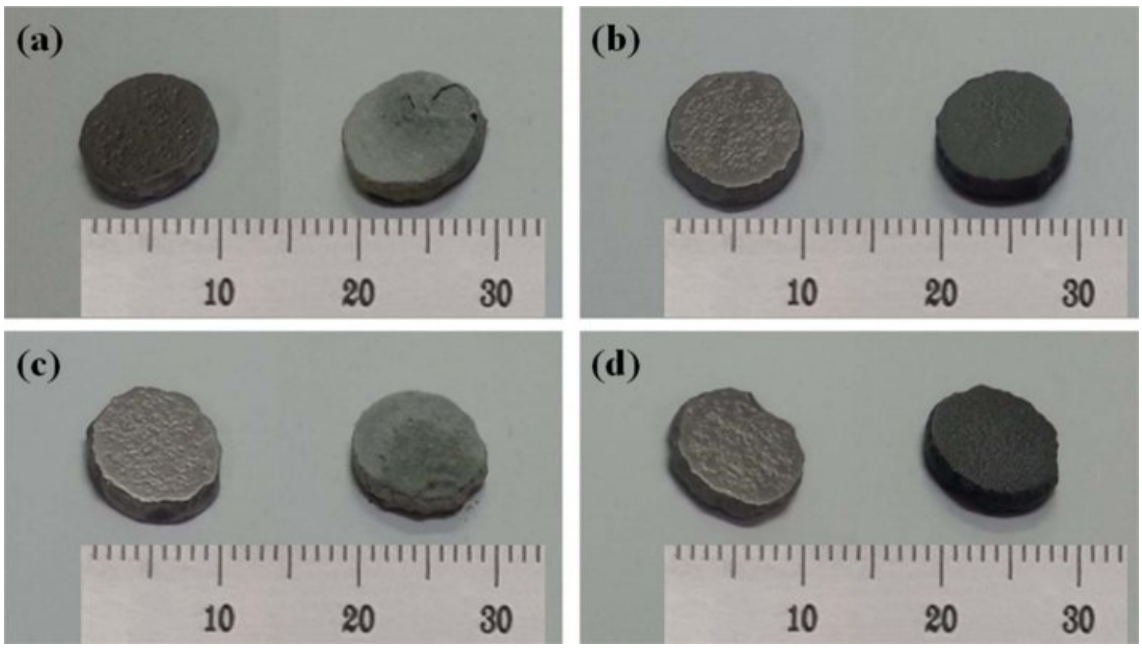

Fig. 2. Photographs of samples: (a) Z, (b) ZS, (c) ZW, and (d) ZSW; before (left) and after (right) torch oxidation.

share main ZrB_2 peaks at 25.2, 32.6, 41.6, 51.7, 58.2, 62.5, 64.4, 68.3, and 74.0°, with each peak corresponding to (001), (100), (101), (002), (110), (102), (111), (200), and (201) planes (JCPDS #34-0423). The composites containing SiC had main peaks of 35.7, 60.1, and 72.0° corresponding to (102), (110), and (116) planes (JCPDS #29-1131). The composites containing WC showed patterns of WB phase with peaks at 39.3, 42.3, and

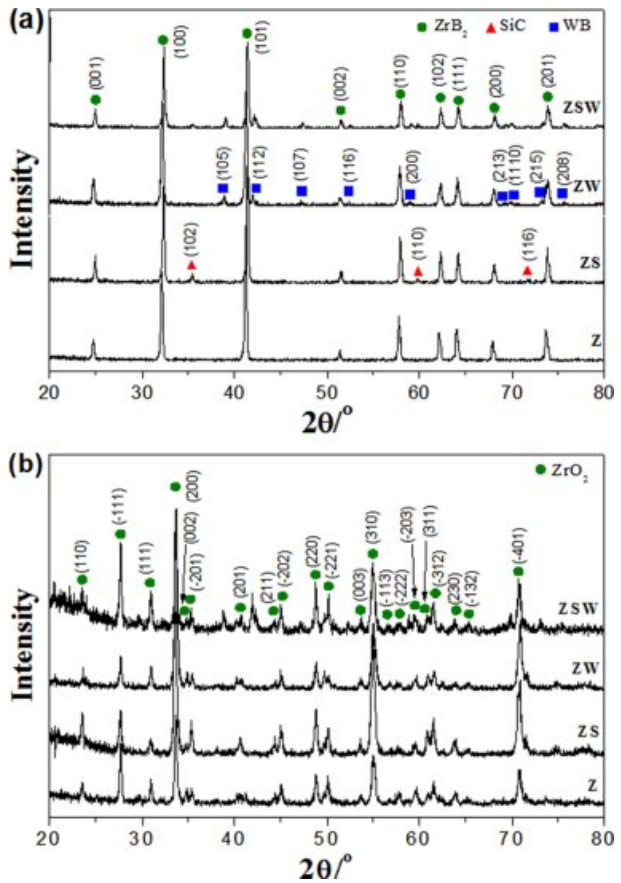

Fig. 3. XRD patterns of samples: (a) before oxidation and (b) after oxidation.

47.5° corresponding to (105), (112), and (107) planes (JCPDS #35-0738). For the ZrB_2-WC composite, a solid solution was formed during sintering, and the excess WC reacted with ZrB_2 to form WB [19]. Fig. 3(b) shows the XRD patterns of four composites after the torch oxidation experiment. ZrB_2 was oxidised into ZrO_2, and peaks of ZrO_2 crystal growth can be seen at 24.0, 28.1, 31.4, 34.2, 49.3, and 50.6°, which correspond to (110), (-111), (111), (200), (220), and (-221) planes (JCPDS #37-1484). Since there are many ZrO_2 phases, i.e. not only for Z but also for ZS, ZW, and ZSW, overlapping makes it difficult to detect peaks of the WO_3 phase at 23.2 and 33.0°.

Cross-sections of the ZrB_2 composites after the torch oxidation experiment were examined through FE-SEM and EDS analysis (Fig. 4, Table 3). The oxidation layer thickness of the cross-section of ZrB_2 composites (Fig. 4(a)) was approximately 49 μm. EDS analysis revealed that the oxidation of ZrB_2 produced a porous ZrO_2 scale on the surface. The structure of the ZrB_2 oxidation layer was columnar, which facilitates the penetration of oxygen and accelerates the oxidation of composites [4-7].

Fig. 4(b) shows the ZrB_2-SiC composites after the torch oxidation experiment. Based on EDS analysis, we can see that the SiO_2 layer is distributed on the surface, and a ZrO_2 layer with hardly any Si is also present. The SiO_2 glass layer appears dense, while the ZrO_2 layer is porous. In fact, composites containing SiC were observed to have shiny surfaces after the oxidation experiment (Fig. 2(b)), which indicates that SiO_2 produced from the oxidation of SiC shifted to the surface. In the cross-section of Sample ZS, the oxidation layer was 29.4 μm thick, among which the borosilicate layer was found to make up 5.31 μm.

The porous layer of the ZrB_2-WC composite shown by FE-SEM was expected to be found, through EDS analysis, to contain ZrO_2 and WO_3. Unlike the ZrB_2-SiC composite, it has a porous oxidation layer but no dense glass layer. However, it is denser than the porous layers shown in Fig. 4(a) and (b). This can be attributed to the blocking of the oxygen path by the porous layer, with volumetric expansion due to the oxidation of WC into WO_3. The oxidation layer thickness was approximately 33.4 μm, lower than that of Sample ZrB_2 but with similar columnar form.

FE-SEM images and EDS analysis of the ZrB_2-SiC-WC composite are shown in Fig. 4(d). SiC formed a dense SiO_2 layer on the surface, while WC was oxidised into WO_3 and caused the middle porous layer to be relatively dense. The XRD results in Fig. 3 show that ZS and ZSW after the torch oxidation experiment had amorphous shapes at approximately 20°. Previously, in the photographs of samples after the torch oxidation experiment in Fig. 2, it was mentioned that borosilicate formed on the surface, which is also consistent with the FE-SEM images. The borosilicate layer was 2.57 μm thick, and the total oxidation layer thickness was 16.9 μm, the thinnest among the four composites. SiC and WC prevented oxidation from accelerating by blocking the path of oxygen.

Fig. 5 shows thermal gravimetric analysis results of ZrB_2, ZrB_2-SiC, ZrB_2-WC, and ZrB_2-SiC-WC composites. Changes in mass were measured while maintaining the temperature at 1,500 °C under atmospheric pressure for 30 min. As can be seen in the TGA graphs, the weight gains of Z, ZS, ZW, and ZSW are 8.2%, 6.8%, 5.3%, and 1.2%, respectively. Oxidation occurred when the samples reacted with oxygen in air, and smaller weight gain indicates lower reactivity. Similar to the results for oxidation layer thickness in the torch oxidation experiment, the weight gain was smallest for the thinnest sample, Sample ZSW. The weight gain of ZS and ZW was 1.4% and 2.9% smaller than that of Z, respectively. This shows that WO_3 oxidised from WC is more effective in blocking the path of oxygen compared with borosilicate obtained from the oxidation of ZrB_2 and SiC. The glass layer of ZSW was 2.57 μm thick, about half that of ZS at 5.31 μm. For Sample ZSW, borosilicate first formed on the surface where oxidation began, and the glass layer blocked the oxygen from entering. The formation of WO_3 helped block the path of oxygen below the surface; SiO_2, which can

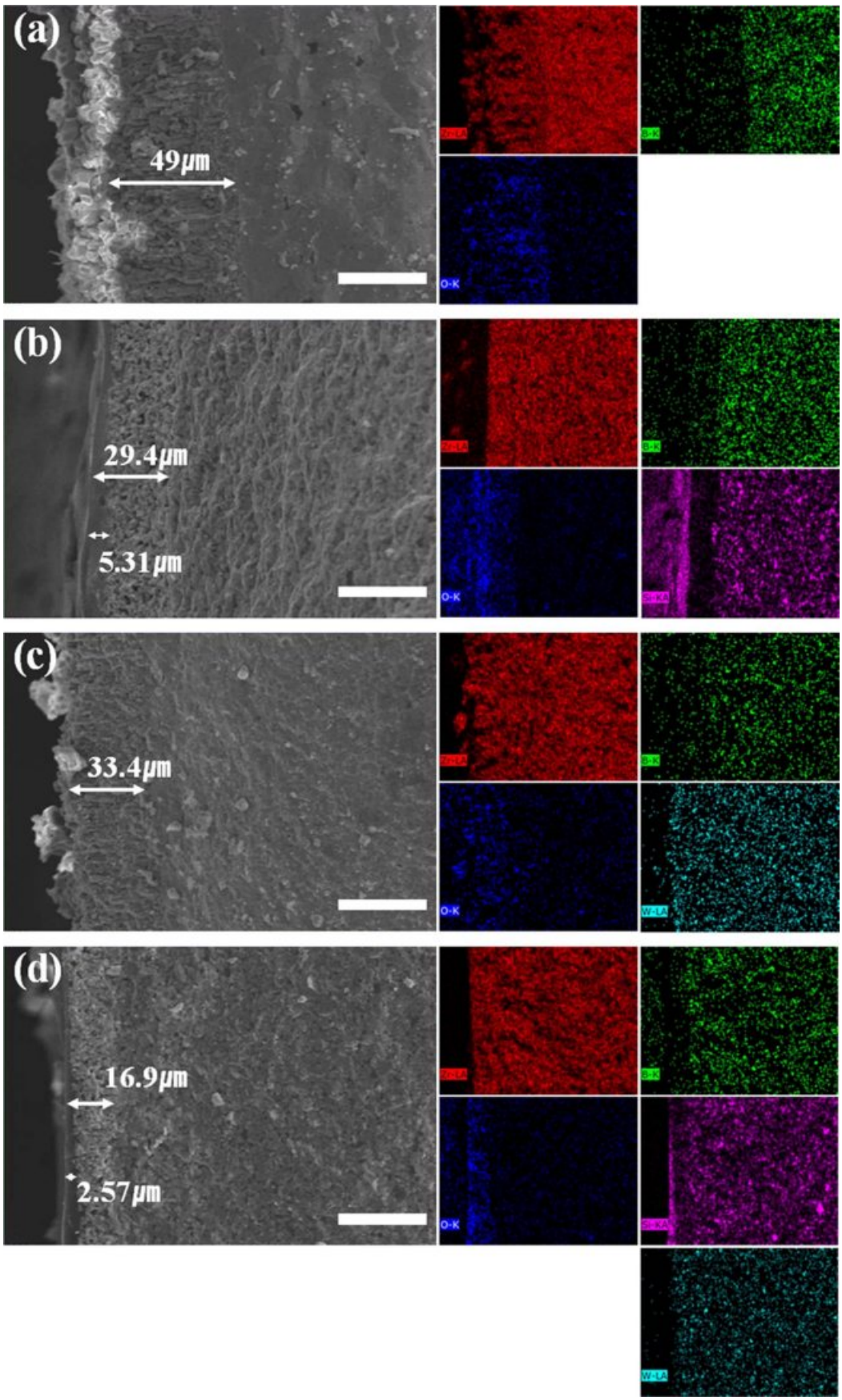

Fig. 4. FE-SEM images and their corresponding EDX elementary images after torch oxidation of samples: (a) Z, (b) ZS, (c) ZW, and (d) ZSW (red: Zr; green: B; blue: O; purple: Si; cyan: W). Scale bar size is 40 μm.

Table 3. Atomic percentage of EDS mapping.

Samples	Atomic percentage (%)				
	Zr	B	Si	W	O
Z	86.0	8.4			5.6
ZS	69.3	7.4	20.7		2.5
ZW	82.1	8.7		6.1	3.2
ZSW	68.2	7.7	16.4	6.5	1.3

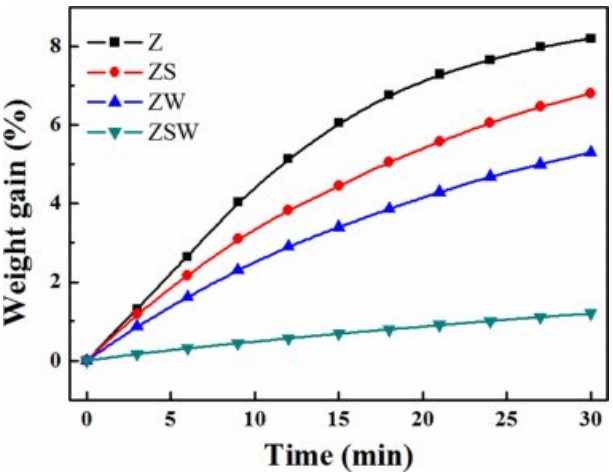

Fig. 5. Weight increases of samples with reaction time at 1,500 °C in ambient atmosphere.

Table 4. Oxidation layers of samples after torch oxidation and TGA.

Samples	After torch oxidation experiment		TGA (%)
	Oxidation layer (um)	Glass layer (um)	
Z	49.0		108.2
ZS	29.4	5.31	106.8
ZW	33.4		105.3
ZSW	16.9	2.57	101.2

exist in liquid phase, blocked the path leading out to the surface. Sample ZSW had a weight gain of 1.2%, comparable to that of Sample Z at 8.2%. TGA analysis shows that oxidation resistance improved significantly. The results are presented in Table 4.

Conclusion

This study sintered ZrB_2-based composites. Spark plasma sintering was employed to sinter poorly-sinterable ZrB_2 composites into composites having a relative density of 98%. SiC and WC are expected to prevent oxidation when sintered with ZrB_2. When the ZrB_2-SiC composite was oxidised, a borosilicate layer developed on the surface, which blocked the path of oxygen and stopped the progress of oxidation. When the ZrB_2-WC composite was oxidised, WC was oxidised into WO_3, leading to an increase in volume. This volumetric expansion was presumed to have further interfered with oxidation by blocking the path of oxygen. Based on the TGA results, the weight gains were 8.2%, 6.8%, 5.3%, and 1.2% for ZrB_2, ZrB_2-SiC, ZrB_2-WC, and ZrB_2-SiC-WC, respectively. In sum, the ZrB_2-SiC-WC composite developed a glass layer on the surface that prevented oxygen from infiltrating, and the oxidised WO_3 prevented SiO_2 leakage while simultaneously blocking the path of oxygen. These factors contributed to significantly enhancing the oxidation resistance of the composites.

Acknowledgments

This work was supported by grants (NRF-2018R1A5 A6075959) from the National Research Foundation of Korea (NRF) funded by the Korean Government and project for ‘New business R&D Voucher’ between Industry, Academy, and Research Institute funded Korea Ministry of SMEs and Startups in 2019. (project No. S2778019).

References

1. S.R. Levine, E.J. Opila, M.C. Halbig, J.D. Kiser, M. Singh, and J. A. Salem, J. Eur. Ceram. Soc. 22[14-15] (2002) 2757-2767.
2. E. Wuchina, E. Opila, M. Opeka, W. Fahrenholtz, and I. Talmy, Electrochem.Soc. Interface, 16 (2007) 30-36.
3. W. G. Fahrenholtz and G. E. Hilmas, NSF-AFOSR joint workshop on future ultra-high temperature materials NSF-AFOSR Draft Workshop Report, National Science Foundation (2004).
4. A.L. Chamberlain, W.G. Fahrenholtz, and Gregory E., J. Am. Ceram. Soc. 89[2] (2006) 450-456.
5. S. Zhu, W.G. Fahrenholtz, G.E. Hilmas, and S. C. Zhang, J. Am. Ceram. Soc. 90[11] (2007) 3660-3663.
6. T.A. Parthasarathy, R.A. Rapp, M. Opeka, and R.J. Kerans, Acta Mater. 55 (2007) 5999-6010.
7. C.R. Wang, J.-M. Yang, and W. Hoffman, Mater. Chem. Phys. 74 (2002) 272-281.
8. F. Monteverde and A. Bellosi, J. Electrochem. Soc. 150[11] (2003) B552-B559.
9. W. C. Tripp and H. C. Graham, J. Electrochem. Soc. 118[7] (1971) 1195-1199.
10. A. Rezaie, W.G. Fahrenholtz, and G. E. Hilmas, J. Eur. Ceram. Soc. 27[6] (2007) 2495-2501.
11. G.-J. Zhang, Z.-Y. Deng, N. Kondo, J.-F. Yang, and T. Ohji, J. Am. Ceram. Soc. 83[9] (2000) 2330-2332.
12. S.S. Hwang, A.L. Vasiliev, and N.P. Padture, Mater. Sci. Eng. A. 464[1-2] (2007) 216-224.
13. J. Han, P. Hu, X. Zhang, and S. Meng, Scr. Mater. 57[9] (2007) 825-828.
14. S. N. Karlsdottir and J.W. Halloran, J. Am. Ceram. Soc. 92[2] (2009) 481-486.
15. W.-M. Guo and G.-J. Zhang, J. Eur. Ceram. Soc. 30[11] (2010) 2387-2395.
16. W.G. Fahrenholtz, J. Am. Ceram. Soc. 90[1] (2007) 143-148.
17. M. Mallik, K.K. Ray, and R. Mitra, J. Eur. Ceram. Soc.

31[1-2] (2011) 199-215.
18. S.C. Zhang, G.E. Hilmas, and W.G. Fahrenholtz, J. Am. Ceram. Soc. 91[11] (2008) 3530-3535.
19. S.K. Choi, S.W. Ui, I.S. Choi, and S.C. Choi, J. Ceram. Soc. Jpn. 122[3] (2014) 198-203.
20. S.C. Zhang, G.E. Hilmas, and W.G. Fahrenholtz, J. Am. Ceram. Soc. 94[4] (2011) 1198-1205.
21. J. Zou, S.-K. Sun, G.-J. Zhang, Y.-. Kan, P.-L. Wang, and T. Ohji, J. Am. Ceram. Soc. 94[5] (2011) 1575-1583.
22. J. Zou, G.-J. Zhang, C.-F. Hu, T. Nishimura, Y. Sakka, J. Vleugels, and O. Van der Biest, J. Am. Ceram. Soc. 95[3] (2012) 874-878.